Elucidating the role of surface passivating ligand structural parameters in hole wave function delocalization in semiconductor cluster molecules

Meghan B. Teunis,[1] Mulpuri Nagaraju,[1] Poulami Dutta,[2] Jingzhi Pu,[1] Barry B. Muhoberac,[1] Rajesh Sardar,[1,4,] and Mangilal Agarwal[1,3,4,]**

[1]Department of Chemistry and Chemical Biology, Indiana University-Purdue University Indianapolis, 402 N. Blackford Street, Indianapolis, Indiana 46202, United States

[2]Department of Chemistry, Michigan State University, 578 South Shaw Lane, East Lansing, Michigan, 48824, United States

[3]Department of Mechanical Engineering, Indiana University-Purdue University Indianapolis, 402 N. Blackford Street, Indianapolis, Indiana 46202, United States

[4]Integrated Nanosystems Development Institute, Indiana University-Purdue University Indianapolis, 402 N. Blackford Street, Indianapolis, Indiana 46202, United States

---

This is the author's manuscript of the article published in final edited form as:

Teunis, M. B., Nagaraju, M., Dutta, P., Pu, J., Muhoberac, B. B., Sardar, R., & Agarwal, M. (2017). Elucidating the role of surface passivating ligand structural parameters in hole wave function delocalization in semiconductor cluster molecules. Nanoscale, 9(37), 14127–14138. https://doi.org/10.1039/C7NR04874B

Corresponding Author

*Rajesh Sardar: rsardar@iupui.edu

*Mangilal Agarwal: agarwal@iupui.edu

One Sentence Summary: An unprecedentedly large bathochromic-shift in the optical absorption band of $(CdSe)_{34}$ SCMs is observed upon passivating their surface with hole delocalizing ligands.

ABSTRACT: This article describes mechanisms underlying electronic interactions between surface passivating ligands and $(CdSe)_{34}$ semiconductor cluster molecules (SCMs) that facilitate band-gap engineering through delocalization of hole wave functions without altering their inorganic core. We show here both experimentally and through density functional theory calculations that the expansion of the hole wave function beyond the SCM boundary into the ligand monolayer depends not only on the pre-binding energetic alignment of interfacial orbitals between the SCM and surface passivating ligands but is also strongly influenced by definable ligand structural parameters such as the extent of their π-conjugation [π–delocalization energy; pyrene (Py), anthracene (Anth), naphthalene (Naph), and phenyl (Ph)], binding mode [dithiocarbamate (DTC, $-NH-CS_2^-$), carboxylate ($-COO^-$), and amine ($-NH_2$)], and binding head group [-SH, -SeH, and -TeH]. We observe an unprecedentedly large ~650 meV red-shift in the lowest energy optical absorption band of $(CdSe)_{34}$ SCMs upon passivating their surface with Py-DTC ligands and the trend is found to be Ph- <Naph- <Anth- <Py-DTC. This shift is reversible upon removal of Py-DTC by triethylphosphine gold(I) chloride treatment at room temperature. Furthermore, we provided temperature-dependent (80-300 K) photoluminescence lifetime measurements, which show longer lifetime at lower temperature, suggesting a strong influence of hole wave function delocalization rather than carrier trapping and/or phonon-mediated relaxation. Taken together, knowledge of how ligands electronically interact with the SCM surface is crucial to semiconductor nanomaterial research in general because it allows the tuning of nanomaterial electronic properties for better charge separation and enhanced charge transfer, which in turn will increase optoelectronic device and photocatalytic efficiency.

Introduction

Quantum confinement of colloidal semiconductor nanocrystals (>2.0 nm in diameter) has generally been controlled through the modification of core size, shape, and composition.[1-6] Long hydrocarbon-containing ligands present in the synthesis are mostly involved in passivating the nanocrystal surface and historically do not play a role in band-gap engineering except to enhance nanocrystal solubility and perhaps photoluminescence (PL) properties. However, these ligands can be substantially varied in structure including their size, chemical composition, and electron donating/withdrawing properties. Recently, Weiss and coworkers reported band-gap modulation of CdSe and CdS nanocrystals by exchanging such hydrocarbon-containing ligands with a ligand that contains a dithiocarbamate (DTC) binding head-group attached to a phenyl ring.[7] The authors deduced that the observed decrease in band-gap resulted from the delocalization of photogenerated exciton (electron-hole pair) hole wave functions from the nanocrystals into its ligand monolayer. The authors modeled wave function delocalization as facilitated by energetic coupling of interfacial orbitals between the nanocrystal and surface passivating ligands, showing that energetic alignment between the highest occupied molecular orbitals (HOMOs) of both nanocrystal and ligand is critical for both maximum delocalization and the largest reduction of band-gaps.[8]

In this article we report a comprehensive study demonstrating that irrespective of the nanocrystal-ligand energy level alignment before binding to the surface, as determined through our density functional theory (DFT) calculations (see **Table S1** and **Fig. S1**), surface ligand structural parameters substantially influence the overall delocalization processes and modulate the band-gap of semiconductor nanocrystals. Our studies show the following: (1) The extent of π-conjugation (π–delocalization energy) within the surface ligand, as exemplified by the series

pyrene (Py), anthracene (Anth), naphthalene (Naph), and phenyl (Ph), is the dominant factor in causing the largest delocalization of the hole wave function and the highest reduction of the band-gap in our $(CdSe)_{34}$ semiconductor cluster molecules (SCMs). (2) The details of surface ligand binding such as attachment mode [monodentate L-type ($-NH_2$) *versus* bidentate chelating, dithiocarbamate ($-NH-CS_2^-$) and carboxylate ($-COO^-$)], and surface binding head group identity (-SH, -SeH, and –TeH) significantly influence the wave function delocalization. The structural diversity of the various ligands used in this present study is shown in **Fig. 1**. Among all the ligand types we studied, our ground-state absorption measurements showed the largest and an unprecedented ~650 meV reduction of band-gap of $(CdSe)_{34}$ SCMs upon post-synthetic ligand exchange of oleylamine (OLA) passivation for Py-DTC (**see Fig. 2**), which was a consequence of delocalization of excitonic hole wave functions. Furthermore, we were able to restore the original band-gap of $(CdSe)_{34}$ SCMs by removing Py-DTC from their surface through treatment with triethylphosphine gold(I) chloride (Et_3PAuCl). Although very recently Buhro and coworkers,[9] and our group[10] reported reversible shifts of optical band-gaps of semiconductor nanocrystals upon treatment with $Cd(carboxylate)_2$ ligands, to the best of our knowledge here is the first example where reversible band-gap modulation is demonstrated for semiconductor nanocrystals functionalized with a series of DTC-type ligands.[7,8,11]

Exciton delocalization is a ground-state electronic phenomenon at the nanocrystal surface-ligand interface in which electron and/or hole wave functions expand beyond the nanocrystal core boundary into either covalently-attached[7,11,12] or electrostatically-interacting ligand monolayers,[9,10] or into adjacent nanocrystals,[13-18] thus decreasing the band-gap of nanocrystals by “increasing the confinement box size”.[19,20] This electronic effect has the potential to increase excited state charge separation and stabilization, thus enhancing excited state charge transfer and

reducing charge recombination rates, which are both ideal for solar fuel generation through water splitting[21-24] and for direct conversion of sunlight to electricity by photovoltaic cells.[25-28] The temperature-dependent excited-state dynamics of semiconductor nanocrystals by which exciton-trap state interactions influence average PL lifetime ($\tau_{\square\square\square}$) is well-studied.[29-33]

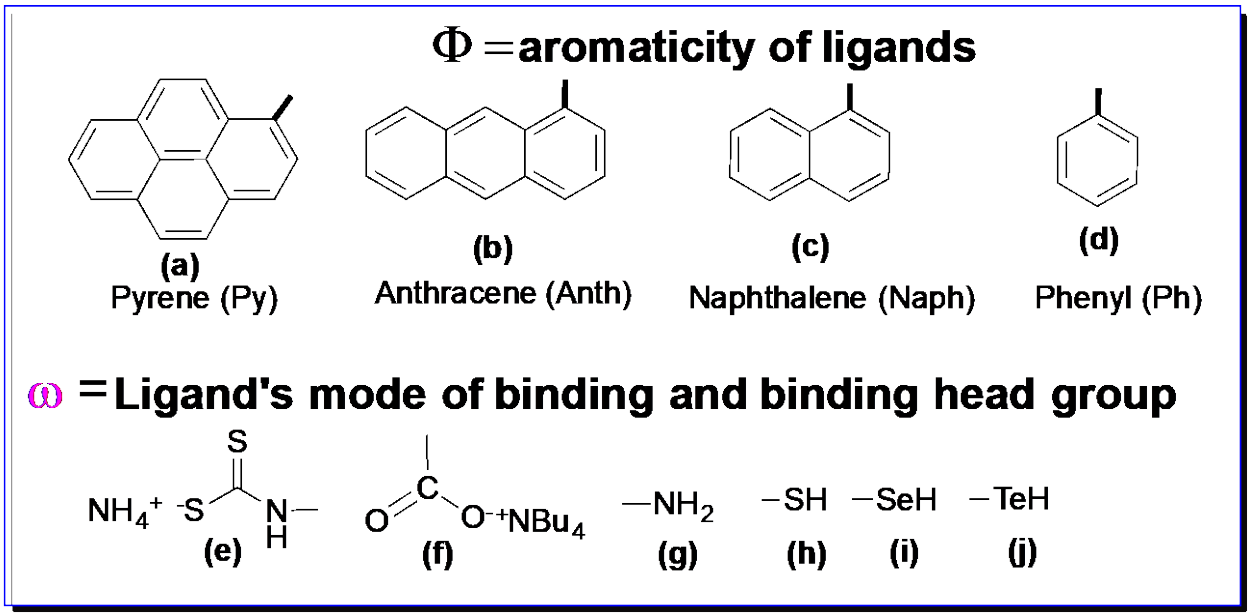

Fig. 1. Chemical structures of ligands showing separate aromatic portions and Cd-binding head groups used in this study. Solid black line represents the point of attachment of ω to Φ.

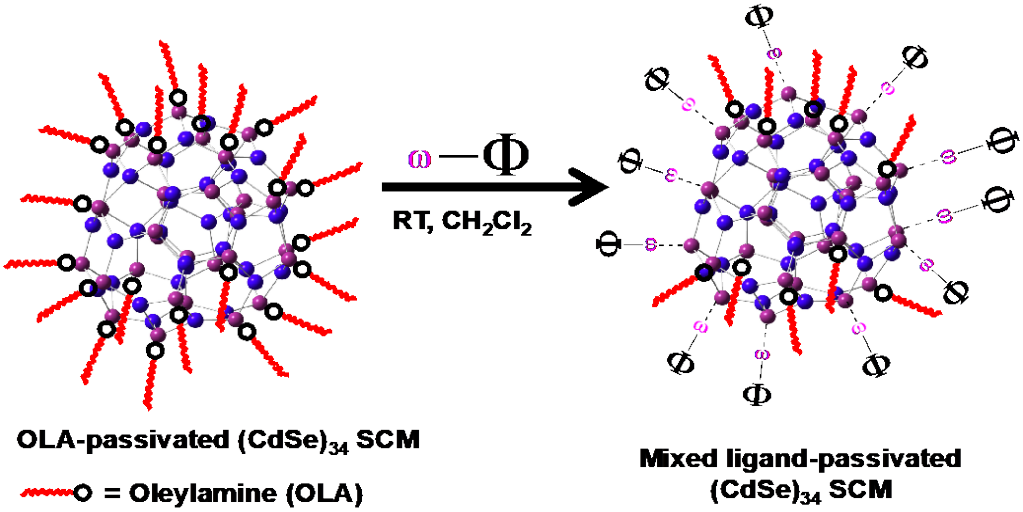

Fig. 2. Schematic diagram depicting post-synthetic ligand exchange of OLA-passivated $(CdSe)_{34}$ SCMs with a generic representation (ω–Φ) of the various ligands shown in Fig. 1. The L-type

ligand OLA preferentially binds with Cd sites. Purple and blue spheres represent Cd and Se atoms, respectively, of the $(CdSe)_{34}$ SCM. The three-dimensional structure of the $(CdSe)_{34}$ SCM does not correspond to the proposed core-cage structure reported in the literature.[34,35] Red wavy lines are the aliphatic chain of OLA with the amine binding head group represented by black circles.

Therefore, we expect that the exciton delocalization process, which is yet to be investigated for ligands with strong hole delocalizing ability, should be temperature dependent. In this article, using time-resolved PL measurements, we demonstrate an ~3.5 fold differences in $\tau_{\square\square\square}$ between 80 and 300 K where the lowest temperature showed the longer $\tau_{\square\square\square}$ values for both Py-DTC- and Naph-DTC-passivated $(CdSe)_{34}$ SCMs. In contrast, Ph-SH-passivated SCMs did not show noticeable changes in $\tau_{\square\square\square}$.

Coupling our research together with knowledge of how coordination chemistry, including the hard-soft acid base (HSAB) principle, guides ligand interactions with SCMs will provide fundamental insights (1) allowing enhancement of characteristics of existing ligand-passivated SCMs and (2) suggesting the design of new ligands to control the band-gap of these hybrid molecules without compromising the inorganic core structure and composition. This unique approach will lay the foundation for preparing artificial solids that have facile charge transport by lowering the inter-cluster tunneling barrier of ligand-passivated SCMs adhered to multilayer films, ultimately increasing the efficiency of solid-state devices. Furthermore, a strong electronic interaction at the SCM-ligand interface is expected to reduce the exciton tunneling barrier[36] and thus facilitate charge separation and extraction, which are critical for SCM photocatalytic applications.[21-24]

Results and Discussion

Since the theoretical crystal structure of the $(CdSe)_{34}$ SCM is known[34,35] and it has a homogeneous surface atom composition (28 Cd and 28 Se), these SCMs form an ideal model system to achieve a principled understanding of the effects of surface ligand attachment onto many types of solid surfaces through determination of the mechanisms underlying electronic interactions between these SCMs and their surface passivating ligands.[37,38] Moreover, the surface ligand interaction has the potential to dramatically alter SCM electronic structure and dictate SCM function more than ligand interactions with larger nanocrystals because smaller SCMs have a greater surface-to-volume ratio that results in a large number of atoms becoming available to interact with the ligands. Our suggestion is supported by dramatic changes in the optical band-gap of $(CdSe)_{34}$ SCMs upon functionalization of their surface with para-substituted Ph-NH-CS_2^- NH_4^+ and Cd(carboxylate)$_2$ ligands[10,39] as compared to larger CdSe nanocrystals under similar experimental conditions.[7,8,40] Moreover, DFT calculations demonstrate that the $(CdSe)_{34}$ SCM possesses a stoichiometric ($Cd_{28}Se_{28}$) composition on its surface. In this context, neutral L-type or anionic X-type ligands will interact electrostatically with surface Cd sites to maintain overall charge neutrality of the $(CdSe)_{34}$ SCM core and provide stability after the post synthetic ligand exchange.[41] Therefore, we would expect to be able to strip off these ligands through treatment with metal complexes where the interaction is stronger in comparison to the original Cd-ligand bond, and thus achieve *reversible band-gap modulation* for X-type exciton delocalizing ligands. Because $(CdSe)_{34}$ SCMs are thermodynamically very stable,[34,35,42,43] no apparent change in their crystallographic structure is expected to take place during such post-synthetic ligand treatment, as we recently demonstrated for Cd(carboxylate)$_2$ treatment of OLA-passivated $(CdSe)_{34}$ SCMs.[10] Finally, the ultra-small size of our SCMs will help maintaining their colloidal stability in

organic solvents upon functionalization with bulky and hydrophobic Py- and Naph-DTCs. In this article, our investigation of surface passivating ligand-controlled hole wave function delocalization is based on the three *hypotheses* listed below:

1) *Ligands bearing larger aromatic π-conjugation (Fig. 1a & b) will result in higher hole wave function delocalization and larger band gap reduction in $(CdSe)_{34}$ SCMs.*
2) *Ligands containing a soft-base, bidentate chelating head group (Fig. 1e) will have stronger interaction with surface Cd^{2+} (soft acid) sites and will result in an increase in interfacial orbital mixing and facile delocalization of $(CdSe)_{34}$ SCMs hole wave functions.*
3) *Ligands containing late row chalcogenide binding head groups (Fig. 1h-j) will create a stronger SCM-ligand interaction and will induce larger exciton $(CdSe)_{34}$ SCMs wave function delocalization.*

Post-Synthetic Surface Modification of OLA-passivated $(CdSe)_{34}$ SCMs with Conjugated DTC-containing Ligands. We selected DTC as the binding head group because bidentate chelating head groups have a thermodynamically favorable complex formation free energy and are expected to display strong electronic interaction with $(CdSe)_{34}$ SCM, as previously reported for large CdSe nanocrystals.[44] To investigate our first hypothesis, we selected Py-, Anth-, Naph-, and Ph-DTC ligands because of their variable extent of π-conjugation. We have previously demonstrated efficient hole wave function delocalization for Ph-DTC-passivated $(CdSe)_{34}$ SCMs where the observed ~510 meV reduction in the band-gap will be used as a reference to examine hypothesis 1.[39] We followed nearly identical post-synthetic surface modification procedures for the various conjugated DTC-containing ligands as was reported earlier by our group and is also

provided in the Electronic Supplementary Information section. **Fig. 3A** illustrates steady-state UV-vis absorption spectra implying the extent of hole delocalization where 650, 620, and 545 meV red-shifts of the lowest energy absorption peak of OLA-passivated $(CdSe)_{34}$ SCMs were observed for Py-, Anth-, and Naph-DTC, respectively. **Table S2** summaries the position of the lowest energy absorption peak (λ) and reduction of confinement energy (ΔE) of OLA-passivated $(CdSe)_{34}$ SCMs before and after functionalization with conjugated DTC-containing ligands. We believe that the observed decrease in $(CdSe)_{34}$ SCM band-gap results from lowering the confinement energy of the SCM-bound hole resulting in delocalization of its wave function into the ligand monolayer through interfacial orbitals, which are formed from the interaction between ligand and SCM. **Fig. 3B** shows changes in the confinement energy of OLA-passivated $(CdSe)_{34}$ SCMs upon functionalization with different DTC-containing ligands.

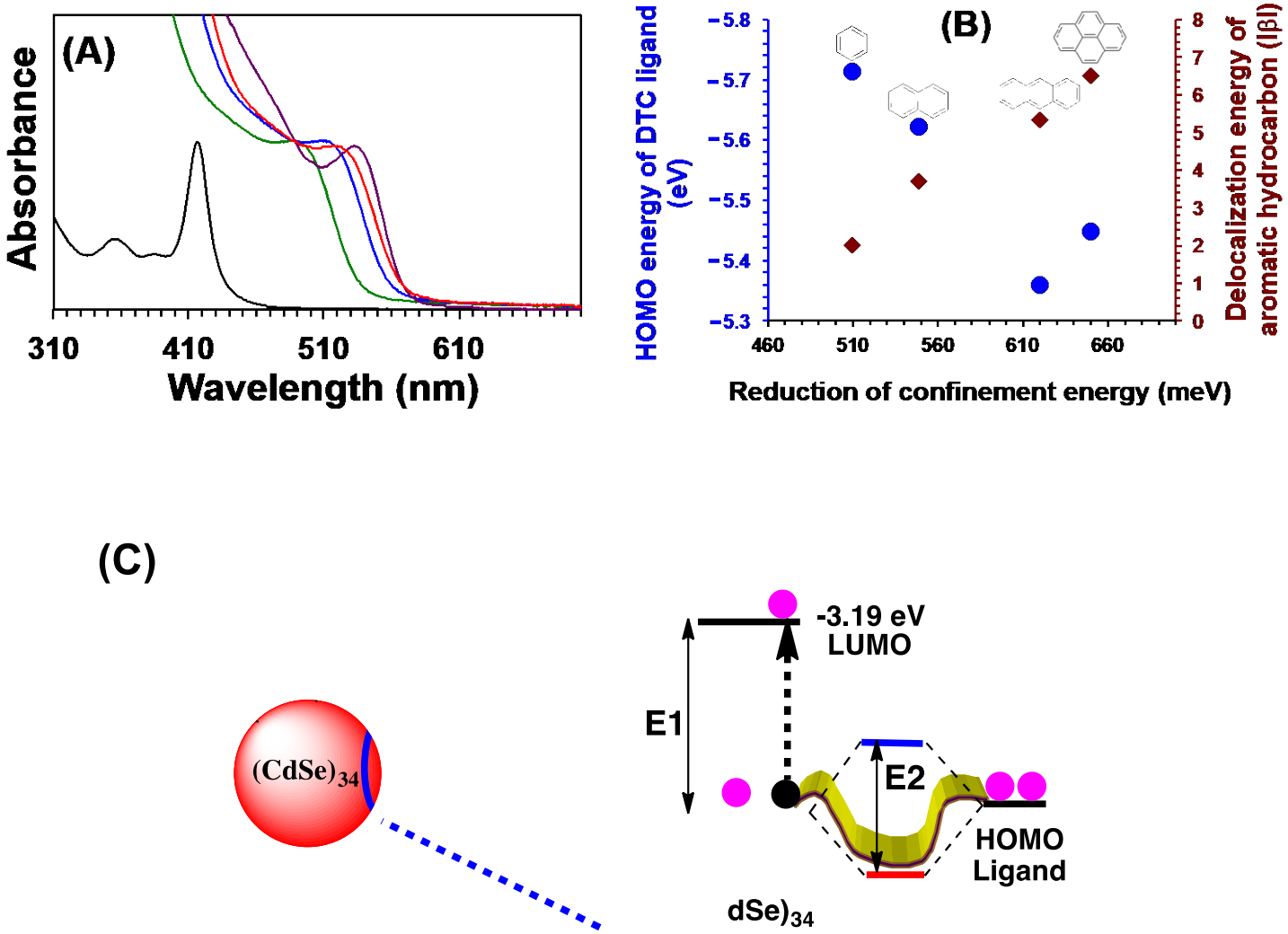

Fig. 3. (A) Room temperature steady-state UV-visible absorption spectra (in CH_2Cl_2) of $(CdSe)_{34}$ SCMs passivated with various π-conjugated DTC type [-NH-CS_2^-] ligands: Ph-DTC (green line), Naph-DTC (blue line), Anth-DTC (red line), and Py-DTC (purple line). The spectrum of Py-DTC-passivated $(CdSe)_{34}$ SCMs was adopted from our published article.[39] The initial OLA-passivated SCM spectrum is shown as a black line. (B) Association of reduction in confinement energy of OLA-passivated $(CdSe)_{34}$ SCMs with the HOMO (blue dots) and delocalization energy (β) (red diamonds) of various aromatic hydrocarbon-containing, DTC-binding ligands that were prepared via exchange reactions. The delocalization energy values of aromatic hydrocarbons were adopted from the literature[45] where |β| = 0.69 eV. (C) Schematic of the various ligand-passivated SCMs. The solid blue ellipsoid highlights the electronic interaction at the SCM-ligand interface. The area inside the ellipsoid represents the bond that is manipulated by varying the chemical structure of ω as shown in Fig. 1 to maximize the electronic interaction of ligand with

surface Cd sites. The Fig. in the blue dotted box represents the molecular orbital diagram of an OLA-passivated $(CdSe)_{34}$ SCM after its interaction with a ligand. Using electrochemistry we determined the HOMO and LUMO energies of a OLA-passivated $(CdSe)_{34}$ SCM at -6.16 and -3.19 eV, respectively with energy gap of E_1.[10] In the excited state, photoexcitation of the SCM creates a hole (black dot) in the HOMO, and thus the SCM can act as a π-acceptor. According to MO theory,[46] this half-filled HOMO can interact with the filled HOMO of the surface passivating ligand (π-donor) and form hybrid bonding (red line) and antibonding (blue line) orbitals with energy gap of E_2. The hybrid bonding orbital facilitates the hole wave function (yellow curve band) delocalization from the SCM to ligand monolayer, thus red-shifting the lowest energy absorption peak because of increase of the size of the confinement box.[10] The image is not to scale.

As reported in literature for large CdSe nanocrystals[7,8] and according to the frontier MO theory,[46] interactions of DTC-containing ligands with a nanocrystal will result in formation of interfacial hybrid orbitals. Such orbitals are expected to reduce the confinement energy of the excitons and facilitate the wave function delocalization with the highest delocalization causing the highest reduction of band-gap. Previously, it was also mentioned that the magnitude of wave function delocalization depends on the energy level alignment between HOMOs of the nanocrystal/SCM and ligands prior to bond formation.[8] Here, better energetic alignment will increase interfacial orbital mixing between these two entities[14] creating stable interfacial orbitals, and thus the hole wave function from the SCM HOMO can delocalize into the hybrid MO and extend the wave function into the conjugated π-system (**Fig. 3C**). We determined the HOMO energies *versus* vacuum (see Table S1) of the ligands using DFT calculations using the basis set 6-311+G** and the B3LYP functional under their optimized geometries in the gas phase. By comparing energy level alignment between HOMOs of the ligands and the $(CdSe)_{34}$ SCM [HOMO energy: -6.16 eV)],[10] Ph-DTC should display the highest reduction of band-gap. However, we observed Py-DTC shows the largest decrease. Therefore, we argue that π–delocalization energy, which follows the highest to lowest order of Ph- <Naph- <Anth- <Py-

DTC in the ligand is the more influential factor rather than energy level alignment. We should also mention that not only energy level matching but also the coupling constant between the orbitals of the SCM and DTC ligands control the overall electronic interaction and formation of hybrid MOs,[46] which facilitate wave function delocalization. In the present investigation, we only considered energy level alignment to explain the changes in the optical band-gap, because to deconvolute complex electronic interactions between the SCM and ligand requires extensive and sophisticated computational calculations[11,47] that are beyond our expertise.

Verifying the effect of the π–delocalization energy, we found that the bidentate chelating moiety of DTC alone is not sufficient to induce a strong SCM-ligand interaction and hole wave function delocalization. To examine this we used aliphatic carbon chain-bearing n-dodecyldithiocarbamate (n-DDTC) to passivate the $(CdSe)_{34}$ SCM surface. UV-vis analysis showed negligible changes in confinement energy (~ 8 meV) (**Fig. S2 and Table S2**), and thus extended exciton delocalization was impossible because of lack of π-conjugation. Furthermore, the DFT-calculated HOMO energy sequence, Ph-DTC < Naph-DTC < n-DDTC < Py-DTC < Anth-DTC, places the aliphatic-containing ligand in-between members of the aromatic sequence. This placement further decouples energy level matching between the ligand HOMO and the SCM HOMO as crucial to reducing confinement energy, with the most influential factor again being the π–delocalization energy that allows efficient delocalization of hole wave functions. Taken together, our selection of surface ligand structural parameters unequivocally demonstrates that the greatest π-conjugation (the largest π–delocalization energy) in the ligand backbone is necessary for the highest delocalization of hole wave functions and the largest reduction of band gap of $(CdSe)_{34}$ SCMs that together validate our hypothesis 1.

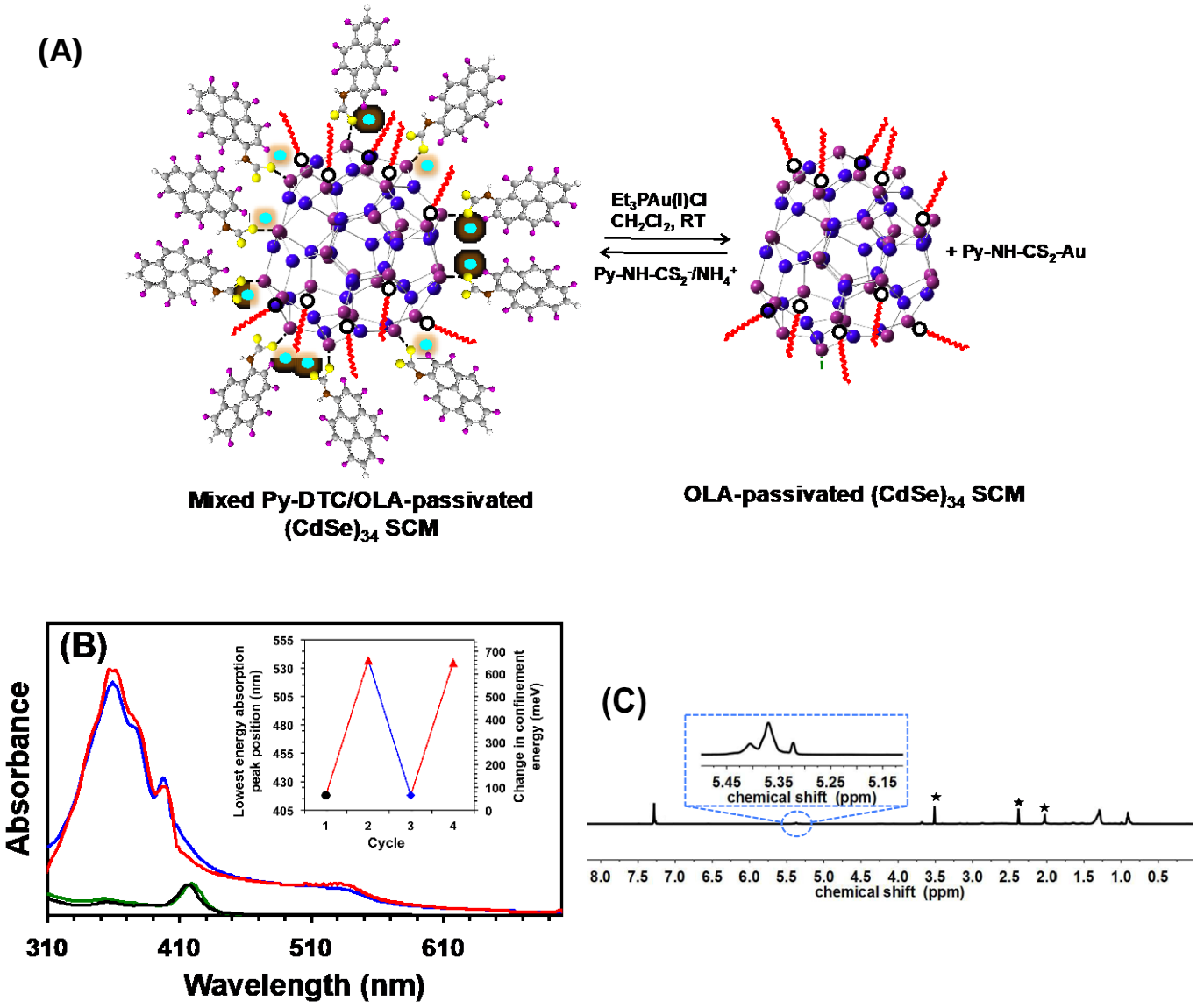

Fig. 4. (A) Schematic diagram represents reversible ligand exchange of a mixed ligand-passivated SCM with Et_3PAuCl. The negatively charged -NH-CS_2^- head group electrostatically interacts with surface Cd site similar to a dative type bond. Purple and blue spheres represent Cd and Se atoms, respectively, of $(CdSe)_{34}$ SCM. Yellow and green spheres are S and N of -NH-CS_2. Pink/light blue dots represent ammonium ion. (B) Steady-state absorption spectra of purified OLA-passivated $(CdSe)_{34}$ SCMs after synthesis (black line), after Py-DTC treatment (mixed Py-DTC-/OLA-$(CdSe)_{34}$ SCMs) (red line), after Et_3PAuCl treatment (partially OLA-passivated SCMs) (green line), and after Py-DTC re-treatment (mixed Py-DTC-/OLA-$(CdSe)_{34}$ SCMs) (blue line). The inset shows reversibility of the lowest energy absorption peak position of OLA-passivated $(CdSe)_{34}$ SCMs (black dot), after repeatedly attaching Py-DTC (red triangles) and removing Py-DTC by Et_3PAuCl treatment (blue diamond). The details of the ligand

treatment and removal are provided in the Materials and Method section. The peaks between 310-410 nm are associated with Py electronic transitions.[48] (C) ^{1}H NMR spectrum of Et_3PAuCl-treated and purified OLA-passivated $(CdSe)_{34}$ SCMs. The expanded vinyl (-CH=CH-) resonance of OLA is shown in the dotted blue box. The asterisks represent signals from residual solvent. The spectrum was collected in $CDCl_3$ at a 15 s relaxation delay time.

Alternatively, one could argue that possible changes in the three following parameters could potentially explain alteration in the band-gap of our SCMs: (i) change in the crystallographic structure,[9] (ii) variation in the number of surface passivating ligands, and (iii) alteration in the core size and/or composition. We performed powder X-ray diffraction analysis of OLA- and Py-DTC-passivating $(CdSe)_{34}$ SCMs in which no noticeable changes in the (100), (002), and (101) reflections of their wurtize crystal structure were observed (see **Fig. S3**).[49] This result suggests that the measured red-shifts in the lowest energy absorption peak of OLA-passivated $(CdSe)_{34}$ SCMs after Py-DTC treatment did not arise from changes in crystallographic structure. To quantify the number of ligands attached to the SCMs surface, we conducted ^{1}H NMR analysis (see **Fig. S4**). The SCMs surface was passivated with both OLA and hole delocalizing ligands where Py-DTC, Anth-DTC, and Naph-DTC were ~60 and ~68, ~68 percent of total surface ligands, respectively. Thus, these treated SCMs contained mixed surface passivation. These data are in agreement with our previous report showing that Ph-DTC treatment caused an ~73 percent exchange of original aliphatic amine ligands. This result is significant and suggested that even though the density (number of ligands/nm^2) of Py-DTC on the $(CdSe)_{34}$ SCMs surface was the lowest, it caused the highest hole wave function delocalization (**see Table S3**).

Based on the NMR analysis, we propose that the negatively charged -NH-CS_2^- binding motif (1) carries ammonium ions (an L-type bound ion-pair) to counter balance the negative charge (2) electrostatically interacts with the surface Cd sites with a dative (coordinate covalent) type bond

(**Fig. 4A**)[40] rather than acting as an X-type ligand involving chelating and bridging interactions with Cd sites (see **Fig. S5**). This particular electronic interaction preserves the overall charge neutrality of the $(CdSe)_{34}$ core. Previously from FTIR analysis we confirmed that OLA-passivated $(CdSe)_{34}$ SCMs do not contain carboxylate type ligands as an impurity on their surface.[10] As illustrated in **Fig. S6**, FTIR analysis of mixed ligand-passivated $(CdSe)_{34}$ SCMs displays both the N-H bending mode of OLA at 1490 cm^{-1} and the asymmetric S-C-S and C-N stretches of Py-DTC at 1024 and 1235 cm^{-1}, respectively. Importantly, no detectable shift in the position of the S-C-S stretch suggests a weak, monodentate-type interaction between the DTC binding motif and surface Cd sites.[50,51] Our proposed coordination chemistry characterizing the ligand interaction with SCMs is different than for previously reported surface DTC-type ligand exchange on Cd-rich semiconductor nanocrystals, where Cd-bound, chelating X-type carboxylate ligands were replaced with X-type DTC-containing ligands forming new Cd-DTC bonds.[7,8,11]

Another possible explanation for band-gap modulation of SCMs upon DTC-type ligand exchange is permanent changes in the inorganic core size and composition. A recent investigation of Ph-DTC exchange with Cd-rich CdSe nanocrystals has suggested that during the exchange reaction, the DTC binding head-group detaches from the Ph ring through decomposition[52] and then sulfur reacts with surface Cd to form CdS that is then deposited onto the CdSe core. This deposition forms CdSe/CdS core-shell type nanocrystals[53] where electron wave function delocalization induces a red-shift in the lowest energy absorption peak. However, such a scenario is very unlikely in our present investigation because $(CdSe)_{34}$ SCM possesses a stoichiometric core (1:1 between Cd-to-Se) and thus formation of a CdS layer would require removal of Se from the core to maintain overall charge neutrality. Under this situation the

original $(CdSe)_{34}$ core size (1.6 nm in diameter)[10] would decrease resulting in a blue-shift of the lowest energy absorption peak, which is opposite to what we have observed. Perhaps one could argue for formation of a $Cd_{34}Se_{34-x}S_x$ alloy SCM during the exchange process, but because of the resulting higher quantum confinement allow SCM would display a larger band-gap than the original $(CdSe)_{34}$ SCM.[54,55] Moreover, our ^1H NMR (**Fig. S4**) and FTIR (**Fig. S6**) analyses unequivocally demonstrated the presence of Py-DTC ligand on the surface of $(CdSe)_{34}$ SCM without any decomposition. Finally "Ostwald ripening," which occurs at temperatures >150 ^oC and requirs addition of Cd and Se precursors,[7] may be another possible explanation for band-gap modulation where some population of $(CdSe)_{34}$ SCMs dissolves to produce monomers that add onto original $(CdSe)_{34}$ SCMs to form larger CdSe nanocrystals via slow growth. However, magic-sized $(CdSe)_{34}$ SCMs are thermodynamically very stable[35,47] and unlikely grow into larger nanocrystals during the ligand exchange reaction. Transmission electron microscopy analysis of our Py-DTC-passivating CdSe nanocrystals showed no change in size maintaining ~1.6 nm average diameter (see **Fig. S7**). Our mixed Py-DTC/OLA-passivated $(CdSe)_{34}$ SCMs displayed their lowest energy absorption maxima at 537 nm (**Fig. 3A**) and CdSe nanocrystals displaying their absorption peak at this wavelength would possess a diameter of ~2.8 nm.[3,7]

Our spectroscopy and microscopy characterizations strengthen hypothesis 1 that the red-shifts in the optical band-gap of OLA-passivated $(CdSe)_{34}$ SCMs upon treatment with conjugated DTC-containing ligands are due to delocalization of hole wave function and not because of change in crystallographic structure, variation in the number of surface passivating ligands, or alteration in the core size and/or composition. A more definitive proof of our hypothesis would stem from demonstration of restoration of the original band-gap of $(CdSe)_{34}$ SCMs by programmable removal of Py-DTC from their surface as similar to an *ion-metathesis* reaction. To

the best of our knowledge such band-gap modulation has not been reported for DTC-containing ligand-passivated semiconductor nanocrystals. As described above, the interaction between the DTC binding group and surface Cd is weak, and thus we expect that a metal ion such as Au(I) would remove Py-DTC from the $(CdSe)_{34}$ SCM surface because of the nearly two fold higher Au-S bond dissociation energy than that of Cd-S.[56] As shown in **Fig. 4A**, we used organically soluble Et_3PAuCl to explore this possibility of Py-DTC removal. **Fig. 4B** shows UV-vis absorption spectra of mixed Py-DTC/OLA-passivated $(CdSe)_{34}$ SCMs before and after treatment with Et_3PAuCl, and then after re-treatment with Py-DTC. The broadening of the absorption peak after removal of Py-DTC could result from some aggregation of SCMs because of the inadequate surface passivation. The shape of the absorption peak was nearly restored after OLA treatment with shape similar to OLA-passivated $(CdSe)_{34}$ SCMs (see **Fig. S8**).

We also performed surface structure characterization of mixed Py-DTC-/OLA-passivated $(CdSe)_{34}$ SCMs after Et_3PAuCl treatment using NMR and energy dispersive X-ray (EDX) spectroscopy. As shown in **Fig. 4C**, no proton signals in the aromatic region (7.9-8.3 ppm) were observed in the ^1H NMR spectrum, suggesting removal of all Py-DTC from the surface of SCMs. More importantly, aliphatic proton resonances associated with Et_3P were not detected. This result was in agreement with the EDX analysis where the P peak at ~2.0 keV did not appear (**Fig. S9**). However, we observed a weak Cl signal at ~2.6 keV that suggests the chloride ions from Et_3PAuCl may have adsorbed onto the surface of $(CdSe)_{34}$ SCM.[57] Taken together, our unique structural characteristics of $(CdSe)_{34}$ SCM allow reversible modulation of hole wave function and confinement energy in which the π-delocalization energy profoundly influences the magnitude of band-gap variation as stated in hypothesis 1.

Effects of Ligand Binding Mode on Band-Gap Modulation of $(CdSe)_{34}$ SCMs. Our observed red-shift of 650 meV in the UV-vis absorption spectra of mixed Py-DTC/OLA-passivated $(CdSe)_{34}$ SCMs was the motivation to explore how the ligand mode of binding influences the overall photophysical properties. DTC is a soft base and according to the HSAB principle, it should demonstrate strong interaction with the soft acid Cd^{2+}. On the other hand, carboxylate ($-COO^-$) and amine ($-NH_2$) are hard bases and thus their interaction with Cd^{2+} is expected to be weaker. Moreover, a recent study[37] shows that the L-type neutral donor ($-NH_2$) interacts more weakly with CdSe nanocrystals than adsorbed ion pairs (e.g., DTC:$-NH-CS_2^-/NH_4^+$ and $-COO^-/Bu_4N^+$). According to hypothesis 2, the stronger the interaction (coupling strength) between the SCM and its ligands, the better the interfacial orbital mixing between them and the higher the delocalization. **Fig. 5** illustrates UV-vis absorption spectra and change in the confinement energy for Py containing ligands with -DTC, $-COO^-/Bu_4N^+$, and $-NH_2$ binding head groups. As expected, mixed Py-COO^-/OLA-passivated $(CdSe)_{34}$ SCMs showed a more than 9-fold smaller change in the confinement energy than Py-DTC/OLA-passivated SCMs, although both of them have chelating bidentate binding ability with Cd^{2+}. **Table S2** summaries the position of the lowest energy excitonic peak (λ) and reduction of confinement energy (ΔE) of OLA-passivated $(CdSe)_{34}$ SCMs both before and after functionalization with Py containing various binding head groups. ^1H NMR analysis confirmed that the surface population of the Py- DTC and Py-COO^- are almost the same (**Table S3**).

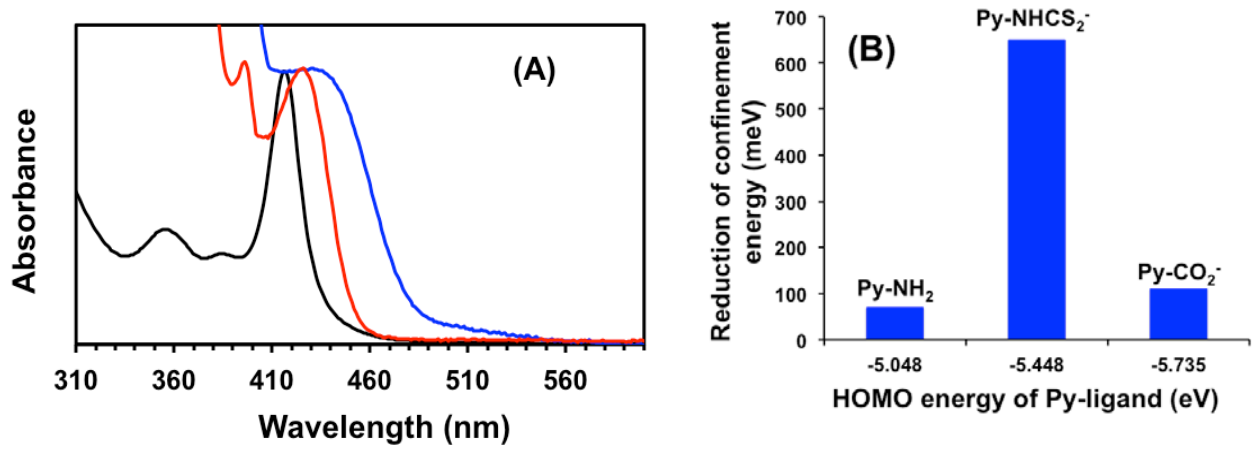

Fig. 5. (A) Room temperature steady-state UV-visible absorption spectra (in CH_2Cl_2) of $(CdSe)_{34}$ SCMs passivated with Py-containing ligands with two different head groups: $-NH_2$ (red line) and $-COO^-$ (blue line). The initial OLA-passivated SCM spectrum is shown in black. (B) Plot of reduction of confinement energy of OLA-passivated $(CdSe)_{34}$ SCMs with respect to the HOMO energy of Py-containing ligands with three different binding head groups that were prepared via ligand exchange reaction.

Moreover, the distances between the Py moiety and surface Cd sites through COO^- and DTC linkages are 4.299 and 5.641 Å, respectively (determined from ChemDraw Professional 15.1, **Fig. S10**). Therefore, the larger change in the confinement energy of Py-DTC/OLA-passivated $(CdSe)_{34}$ SCMs cannot be explained by a longer DTC to Cd separating distance. Mixed Py-NH_2/OLA-passivated $(CdSe)_{34}$ SCMs displayed the smallest absorption peak red shift of 70 meV. This result is in agreement with a recent study[37] showing the L-type neutral donor ($-NH_2$) more weakly interacting with CdSe nanocrystals than the adsorbed ion pairs (e.g., $-NH-CS_2^-/NH_4^+$ and $-COO^-/Bu_4N^+$). Nevertheless, our investigation has shown that not only the π-delocalization energy is important for effective delocalization of hole wave functions but ligand mode of binding is also critical.

Effects of Ligand Binding Head Group on Confinement Energy of $(CdSe)_{34}$ SCMs. Based on the HSAB principle, Cd-binding ligands containing the hard $–NH_2$ binding head group favor replacement with soft groups such as chalcogenides. The strength of interaction between the SCM and ligand will influence SCM interfacial orbital mixing and confinement energy, and will control hole wave function delocalization. We selected the head group series Ph-EH (E = -S, -Se, and -Te) to validate our hypothesis 3. **Fig. 6A** shows UV-vis absorption spectra of three different chalocogenide ligand-passivated $(CdSe)_{34}$ SCMs where the reduction in ΔE is as follows: Ph-SH (136 meV) < Ph-SeH (200 meV) < Ph-TeH (211 meV). **Table S2** summaries the corresponding λ position. EDX analysis confirmed the formation of mixed Ph-E-/OLA-passivated SCMs (**Fig. 6B**). The number of ligand attached to the surface of $(CdSe)_{34}$ SCMs was determined from ^1H NMR analysis (data not shown). Importantly, the largest shift we observed is 6.5 fold greater than the previously reported value by Brutchey and coworkers for the same ligand system using 4.0 nm diameter CdSe nanocrystals.[12] By considering the energy level alignment between HOMOs of $(CdSe)_{34}$ SCM and Ph-E ligands the order should be Ph-TeH < Ph-SH ≈ Ph-SeH (see **Table S2**). However, we observed a completely different order as shown above. Therefore, the magnitude of decrease in the confinement energy of $(CdSe)_{34}$ SCMs upon treatment with Ph-E followed the HSAB principle. We believe that the energy level alignment between the SCM and ligand HOMOs is not close enough for the relaxation of quantum confinement but the strength of the interaction, which is be guided by the HSAB principle, plays a vital role.

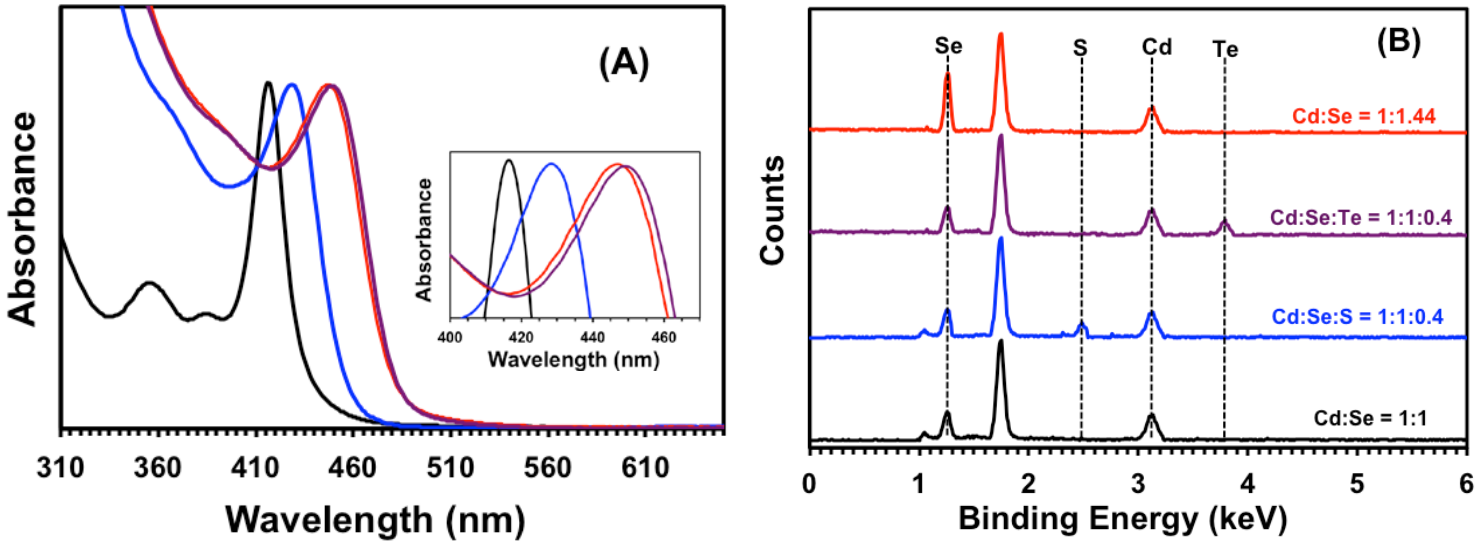

Fig. 6. (A) Room temperature steady-state absorption spectra (in CH_2Cl_2) of SCMs with various surface passivation: Singly $(OLA)_{19}$-passivated $(CdSe)_{34}$ SCMs (black line), and mixed $(Ph\text{-}SH)_{14}$-/$(OLA)_5$- (blue line), $(Ph\text{-}SeH)_{15}$-/$(OLA)_4$- (red line), and $(Ph\text{-}TeH)_{15}$-/$(OLA)_4$-passivated (purple line) $(CdSe)_{34}$ SCMs. Number of OLA per $(CdSe)_{34}$ SCM was reported in the literature.[10,58] The inset shows expanded region of the lowest energy excitonic transition. (B) EDX profile of various ligand-passivated $(CdSe)_{34}$ SCMs. The spectra are color matched to those in (A). The appearance of S and Te originates from the Ph-SH and Ph-TeH ligands while the Ph-SeH ligand treatment increases the Se content in the sample.

Steady-State and Time-Resolved Photoluminescence (PL) Properties of Conjugated DTC-Containing Ligand-Passivated $(CdSe)_{34}$ SCMs. We examined the hole wave function delocalization of $(CdSe)_{34}$ SCM into the ligand monolayer by characterizing the samples with steady-state PL spectroscopy. The PL spectra of conjugated ligands containing the DTC binding head group exhibited almost 95% quenching of PL peak intensity (**Fig. 7A**), which is consistent with the literature reports on DTC-containing ligands.[7,11,12] It is known that the attachment of thiols through Cd-thiolate (Cd-S-) covalent linkage creates hole-trapping sites in Cd-chalcogenide nanocrystals[59,60] that result in non-radiative recombination of excitons and

quenching of PL intensity. Although in our system no covalent Cd-S linkage was formed, the delocalization of the hole wave function still reduced the maximum probability of radiative recombination of exciton wave functions. We were unable to quantify the reduction of confinement energy from the PL measurements because of the overlapping optical peak position of conjugated DTC ligands and $(CdSe)_{34}$ SCMs. As shown in **Fig. 7B**, strong PL quenching for Ph-EH ligands was also observed. Importantly, we were able to calculate the reduction of confinement energy from the PL peak position for mixed Ph-EH-/OLA-passivated $(CdSe)_{34}$ SCMs (**Fig. 7B, inset**). These data nicely corroborate our UV-vis absorption measurements and support the hole wave function delocalization mechanism.

In order to examine the mechanism of hole wave function delocalization, we characterize three different samples by temperature-dependent (85-300 K), time-resolved PL spectroscopy. At 300 K mixed Py-DTC-/OLA-, Naph-DTC-/OLA- and Ph-SH-/OLA-passivated $(CdSe)_{34}$ SCMs displayed τ_{avg} values of 27.9, 19.6, 3.9 ns, respectively, whereas singly OLA-passivated SCMs showed τ_{avg} of ~22 ns (**see Fig. 7C and Table S4**). The shortening of τ_{avg} after either Naph-DTC or Ph-SH ligand passivation could be from a combined effect involving trap state- and hole delocalization-mediated recombination of excitons in which the presence of surface traps reduces τ_{avg} but the delocalization process increases the $\tau_{avg.}$[10,61-64] The slight increase in τ_{avg} for Py-DTC-/OLA-passivated $(CdSe)_{34}$ SCMs is an indication of relative weaker overlap between electron and hole wave functions, as a consequence of hole wave function delocalization, in comparison to singly OLA-passivated SCMs. We believe for Py-DTC-/OLA-passivated $(CdSe)_{34}$ SCMs, hole wave function delocalization is the dominant factor rather than trap-state mediated excitonic recombination. However, quantifying the precise contribution for each quantity is difficult under our experimental conditions. Interestingly, the τ_{avg} values determined for our three above-

mentioned ligand-passivated SCMs are much higher than the previous report by La Croix et al.[11] and Brutchey and coworkers[12] where the authors suggested a hole transfer mechanism rather than the excited state hole delocalization process. Moreover, in these reports a significant reduction in τ_{avg} was observed after attachment of hole delocalizing ligands. However, according to the literature report as mentioned above, exciton wave function delocalization is expected to increase the τ_{avg} unless a trap-state mediated excitonic recombination takes place.

Our low temperature time-resolved PL measurement show three important excited state dynamic characteristics: Firstly, the fast relaxation component (τ_1) is present both at room temperature and at 80 K for all three above-mentioned hole delocalizing ligands (**see Table S4**). Moreover, τ_1 values determined for all three ligands at five different temperatures are all the same within experimental error. Therefore, in our system phonon-assisted relaxation can be eliminated because under such circumstances, τ_1 should not be observed at 80 K.[12] The biexponential decay observed with τ_1 can be described as decay of bright excitons before reaching thermal equilibrium between bright and dark emitting states.[31] Secondly, as illustrated in **Fig. 7D**, mixed Ph-SH-/OLA-passivated $(CdSe)_{34}$ SCMs showed nearly identical decay values for the slow component (τ_2) at different temperatures. It has been determined experimentally that the τ_{avg} of semiconductor nanomaterials is temperature independent up to room temperature because exciton localization takes place as a consequence of the presence of trap states.[65,66] This concept is in agreement with our findings in that we believe trap-state mediated PL properties are more dominant than delocalization processes in Ph-SH-/OLA-passivated $(CdSe)_{34}$ SCMs. Thirdly, both Py-DTC-/OLA- and Naph-DTC-/OLA-passivated $(CdSe)_{34}$ SCMs displayed strong temperature-dependent dynamics in which τ_2 and τ_{avg} increased with decreasing temperature. These long-lived, biexponential excited state time constants indicate the presence of a highly

delocalized spatial distribution of excitonic wave functions around the SCMs and that the effects of carrier trapping are negligible.[32] We did not investigate the excited state dynamics at temperatures <80 K because in ultrasmall SCMs, the delocalization process can be masked by bright-dark splitting, which increases as size decreases.[67] Taken together, this ligand-controlled, temperature-dependent study indicates that the exciton delocalization process in ultrasmall SCMs strongly influences their excited state dynamics.

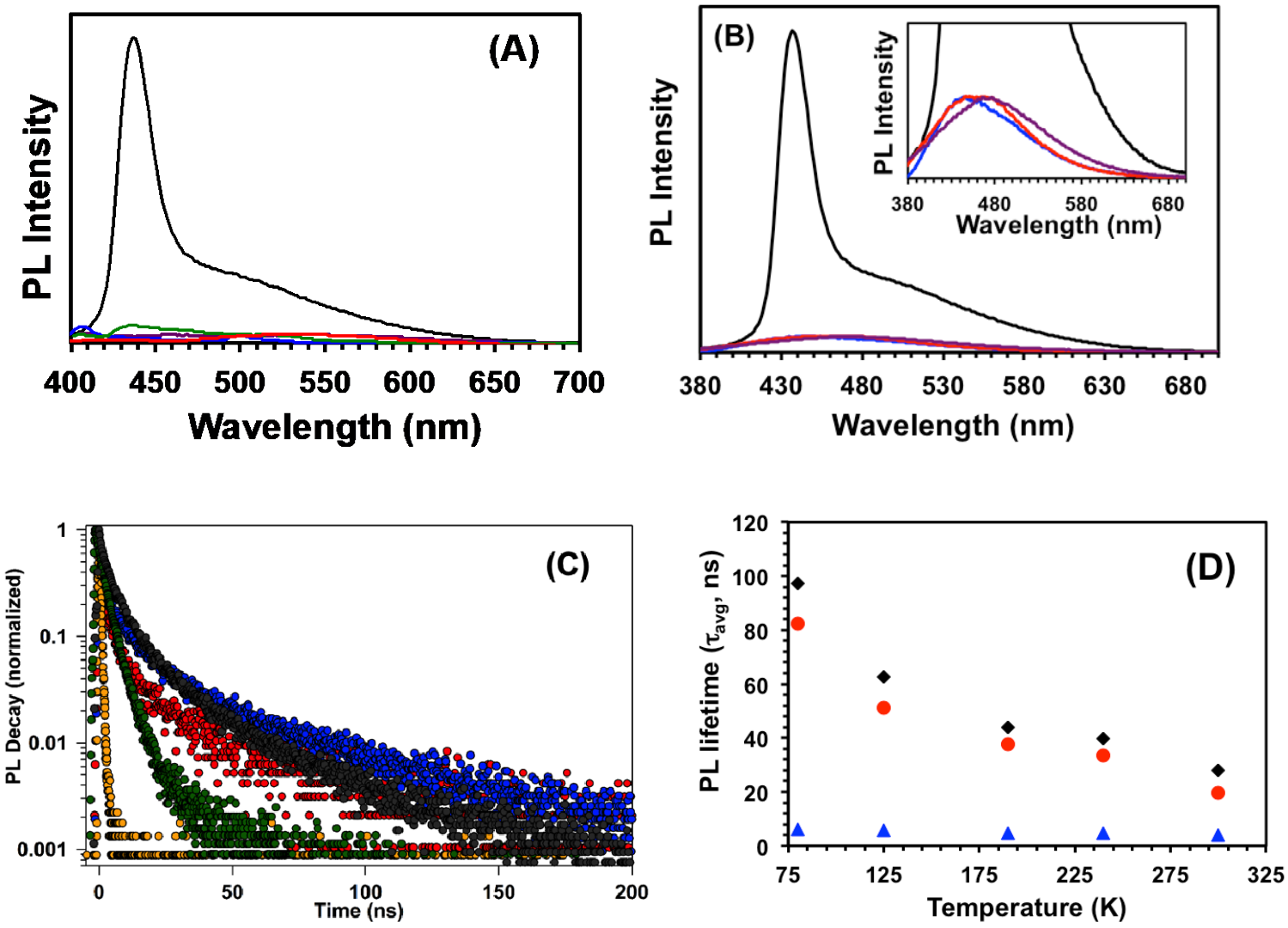

Fig. 7. Room temperature steady-state PL spectra (in CH_2Cl_2) of various π-conjugated DTC type ligand-passivated $(CdSe)_{34}$ SCMs: Ph-DTC (green line), Naph-DTC (blue line), Anth-DTC (red line), and Py-DTC (purple line). (B) Room temperature steady-state PL spectra of only OLA-passivated (black line), and mixed Ph-SH-/OLA- (blue line), Ph-SeH-/OLA- (red line), and Ph-TeH-/OLA-passivated (purple line) $(CdSe)_{34}$ SCMs in CH_2Cl_2. The PL spectra were collected at 350 nm excitation energy. The inset shows an expanded region of the mixed Ph-EH-/OLA-passivated $(CdSe)_{34}$ SCMs. PL spectrum of original OLA-passivated SCMs is shown by a black line in both panel (A) and (B). (C) Typical time-resolved PL traces measured at 300 K for different ligand-passivated $(CdSe)_{34}$ SCMs: mixed Py-DTC-/OLA- (blue dots), mixed Naph-DTC-/OLA- (red dots), and mixed Ph-SH-/OLA-passivated (green dots) SCMs, and the original OLA-passivated SCMs (black dots). All spectra were normalized to 1.0. The instrument response function (IRF, yellow dots) of this system was measured as 0.4 ns. (D) Temperature dependence of τ_{avg} for Py-DTC-/OLA- (black diamonds), Naph-DTC-/OLA- (red dots), and Ph-SH-/OLA-passivated (blue triangles) SCMs.

Conclusions

In conclusion, we have shown that the excitonic confinement energy of $(CdSe)_{34}$ SCMs can be reversibly manipulated – up to a 650 meV shift in the lowest energy excitonic peak – by post synthetic ligand exchange through controlling delocalization of SCM hole wave functions into interfacial electronic states. We determined that delocalization of hole wave function is predominantly controlled by a combination of extended π-conjugation (highest shift for Py) and binding head group (highest shift for DTC) of surface passivating ligands rather than by energy level alignment between the HOMOs of SCM and ligand. Thus, the strength of the electronic interaction between SCMs and their surface passivating ligands is governed by coordination chemistry and the HSAB principle. Moreover, our steady-state and time-resolved PL studies confirm that hole wave function delocalization weakens electron-hole recombination ability resulting in a relative increase in PL lifetime as compared to the original OLA-passivated $(CdSe)_{34}$ SCMs before ligand exchange. Furthermore, our temperature-dependent PL characterization suggests that carrier trapping and/or phonon-mediated relaxation does not play a role in determining τ_{avg} however a strong influence by hole wave function delocalization was observed, and this provides a comprehensive study of hole delocalizing ligand-passivated semiconductor nanocrystals in general.

The interfacial electronic interaction produces strongly coupled SCM-ligand hybrid molecules, which have tremendous potential in providing a wealth of information on physicochemical, photophysical, and electrochemical properties at the molecular level that can be used to maximize charge transfer and transport efficiencies. Despite their potential for

providing valuable molecular level information, current ligand-coated CdSe SCMs display band-gaps >2.90 eV[34,35,49] in the blue region of the solar spectrum. This size gap makes them unsuitable for effective solar-based energy production, which requires visible to near infrared band-gaps. Based on this current work, we predict that an extension of band-gap range for ultrasmall CdSe SCMs can be achieved through the appropriate selection of surface ligand chemistry without compromising their core diameters or compositions, thus enhancing their potential application as photocatalysts. In addition, Py is known to undergo π-stacking by itself or with graphene and carbon nanotubes, and thus there can be p-orbital overlap and an increase in carrier diffusion length, resulting in facilitation of charge transport for photodetector applications.[68]

Using transient absorption (TA) spectroscopy, we were the first to report ultrafast hole transfer of $(CdSe)_{34}$ SCMs that were functionalized with the hole delocalizing ligand, Ph-DTC.[69] A recent report by Lian et al.[70] supports our original finding that the existence of exciton delocalization in semiconductor nanocrystals facilitates the extraction of charge carriers. Our current work presenting a comprehensive study on selection of the best hole wave function delocalizing ligand should further enhance TA studies investigating hole transfer from nanocrystals to their ligand monolayer. Moreover, we recently reported the electron wave function delocalization ability of $Cd(carboxylate)_2$ ligands.[10] Taken together, functionalization of $(CdSe)_{34}$ SCMs with dual hole and electron delocalization ligands should provide a rational approach for efficient extraction of both types of charge carriers and is a logical step for future time-resolved excited-state PL and TA spectroscopy studies.

Experimental Section

Materials. Cadmium acetate ($Cd(OAC)_2$, 99.9%), selenium (pellets, 99.9%), oleylamine (OLA, 70%), dodecylamine (DDA, >99%) 1-hexanethiol (HT, 95%), 1-aminopyrene (Py-NH_2, 97%), 1-aminoanthracene (Anth-NH_2, 90%), 1-naphthylamine (Naph-NH_2, 99%), 1-pyrenecarboxylic acid (Py-COOH, 97%), thiophenol (Ph-SH, 99%), benzeneselenol (Ph-SeH, 97%), diphenditelluride (Ph-TeH, 97%), triethylphosphine gold (I) chloride (Et_3PAuCl, 99.9%), tetrabutylammonium hydroxide (Bu_4NOH, 98%), toluene (HPLC grade), acetonitrile (CH_3CN, HPLC grade), chloroform ($CHCl_3$, HPLC grade), sure seal methylene chloride (CH_2Cl_2, HPLC grade, >99%), carbon disulfide (CS_2, 99.9%), concentrated ammonium hydroxide (NH_4OH, ACS grade) were purchased from Sigma-Aldrich and used without further purification. Organic solvents were purged with N_2 for 30 min prior to use. NMR solvents were dried over molecular sieves prior to use. All surface modifications and NMR sample preparation were performed inside a N_2-filled glovebox.

Absorbance, Steady-State Photoluminescence (PL), Temperature-Dependent PL Decay, NMR, and FTIR Spectroscopy, and Electron Microscopy Measurements. UV-vis absorption spectra were collected using a Varian Cary 50 UV-vis spectrophotometer over a range of 800-300 nm. Prior to sample measurement, the baseline was corrected using pure solvent. The emission spectra were acquired using a Cary Eclipse fluorescence spectrophotometer from Varian Instruments. ^1H NMR was recorded on a Bruker AVANCE III 500 instrument at 500 MHz frequency. Approximately ~10 mg of SCMs were dissolved in 0.6 mL of CD_2Cl_2 at room temperature and a minimum of 1000 scans were collected. A 15 s relaxation delay time was used, which is considered to be sufficient for accurate integration of the aromatic peak region. FTIR spectra were acquired using a Thermo Nicolet IS10 FTIR spectrometer. For FTIR analysis, samples were prepared using a 1:10 ratio of sample to KBr, ground using a mortar and pestle, and pressed into a pellet. A minimum of 300 scans were collected and all data were processed using Omnic FTIR software. The lifetime measurements were recorded using a time-correlated single-photon counting (TCSPC) set up. The data acquisition card (DAQ) was from Edinburgh Instruments (TCC900). The laser used for the experiment is a 405 nm pulsed laser from Picoquant (LDH-D-C-405M, CW-80 MHz). The detector was a photomultiplier tube (PMT) from Hamamatsu (H7422-40). For the temperature dependent PL decay measurements, the $(CdSe)_{34}$ SCMs solution was placed inside an EPR tube and then the tube was mounted onto the probe using a cryogenic laboratory tape and introduced into a continuous-flow cryostat (Janis Research Company). The temperature was varied from 80 K to 300 K (liquid N_2 cooling) and was controlled using a temperature controller (Lake Shore 335). As the desired temperature was reached, the SCM solution was set at that particular temperature for 15 min to attain thermal equilibrium before measuring the PL decay. TEM analysis was conducted in a Technai-12 instrument operating at 120 kV.

Synthesis of OLA-Passivated $(CdSe)_{34}$ SCMs. OLA-passivated $(CdSe)_{34}$ SCMs were synthesized using our published procedure with minor modifications.[49] Briefly, 0.2 g of $Cd(OAc)_2 \cdot 2H_2O$ was dissolved by stirring in 5 mL of OLA in a 100 mL two-neck round bottom flask at room temperature under reduced pressure. The Se precursor was prepared by adding 0.12 g of freshly ground selenium powder to a 5 mL round bottom flask containing 1.57 mL OLA and 0.430 mL of HT under N_2 atmosphere and stirred until all the Se was dissolved. Once a clear

solution of Cd salt was achieved, 5 mL toluene was added to the reaction mixture. Then 1 mL of the freshly prepared Se precursor was added to the mixture and it was stirred for 24 h under N_2 atmosphere. The SCM growth was quenched by diluting with 20 mL of hexane and adding a mixture of CH_3CN/CH_3OH (1:1 v/v) dropwise until the solution became cloudy. The solution was then centrifuged at 7000 r.p.m. for 5 min yielding a yellow solid. The purification step was repeated an additional two times to remove free ligand. The resulting SCMs were used in the present investigation.

Synthesis of Py- Anth-, Naph-DTC. Py-DTC, Anth-DTC, and Naph-DTC were prepared according to a literature procedure, as similar to Ph-DTC.[71] Briefly, 82.0 mmol of CS_2 was added drop-wise over 30 min to 41.0 mmol of either Py-NH_2, Anth-NH_2, or Naph-NH_2 dispersed in 30 mL of concentrated NH_4OH at 0 °C. The solution was stirred under N_2 overnight. The products were washed with cold chloroform and dried under vacuum overnight. The product was recrystallized by maintaining the solution at -20^{O} C for 48 h. All products were characterized by ^{1}H NMR spectroscopy and electrospray ionization-mass spectrometry. We followed the same experimental method to prepare n-DDTC. All the ligands were stored inside a N_2-filled glovebox at -35 ^{0}C.

Ligand Exchange Reaction. All samples were prepared inside a nitrogen-filled glovebox in dark and reactions were carried out in a Schlenk line. A 0.19 mmol quantity OLA-passivated $(CdSe)_{34}$ SCM was dissolved in 1:9 $CHCl_3$:CH_2Cl_2 (total 10 mL) in a 25 mL two neck round bottom flask followed by addition of 0.39 mmol of Py-DTC ligand. Since Py-DTC ligand was not soluble in DCM, the biphasic reaction mixture was vigorously stirred at room temperature for 48 h. The exchange reaction was monitored by removing 200 μL of the reaction mixture and then centrifuging to remove insoluble solid while determining the lowest energy peak position. 100 μL of the colored supernatant was then diluted into 3-mL of DCM for UV-vis spectroscopic characterization. After the reaction mixture displayed a stable lowest energy absorption maximum, it was centrifuged, dried under reduced pressure, and stored inside a glovebox. The Py-DTC-passivated $(CdSe)_{34}$ SCM were completely soluble in DCM. We followed a similar ligand exchange procedure for other DTC-containing ligand types. Py-carboxylic acid was deprotonated with tetrabutylammonium hydroxide prior to use.

Modification of Py-DTC –Passivated* (CdSe)$_{34}$ SCMs *Through Surface Ligand Removal by Et_3PAuCl. A 0.02 mmol quantity of Py-DTC-coated $(CdSe)_{34}$ SCMs was dissolved in 5 mL of CH_2Cl_2. Next, 0.5 mmol of solid Et_3PAuCl was added to the solution and stirred vigorously for 24 hr at room temperature. The solution was centrifuged at 7000 rpm for 5 min, the supernatant was discarded, and the yellow solid was collected. The solid was then dissolved in toluene and the solution was centrifuged at 5000 rpm for 2 min to remove insoluble Py-DTC-Au complex while saving the supernatant, which was partially passivated $(CdSe)_{34}$ SCMs, for further characterization. To reestablish the complete solubility of $(CdSe)_{34}$ SCMs in $CHCl_3$, 0.06 mmol of OLA was added and stirred for 6-8 hr at room temperature. The SCMs were then precipitated with CH_3OH to remove any excess OLA. This fully OLA-passivated $(CdSe)_{34}$ SCM sample was now used for second cycle reversibility studies.

Theoretical Calculation of HOMO and LUMO Energy Position of Ligands. Orbital energy calculations (see Table S1) were performed with QChem 3.1 software using a basis set of 6-311+G** and B3LYP functional.

Electronic Supplementary Information. UV-visible absorption, PL, ^{1}H NMR, XRD, EDS, and FTIR spectra; a TEM image of mixed Py-DTC-/OLA-passivated $(CdSe)_{34}$ SCMs; tables of HOMO and LUMO energies of ligands; and temperature dependent PL decay constants.

ACKNOWLEDGMENTS

The experimental work is supported in part by IUPUI-OVCR (R.S) and IUPUI start-up funds (M.A). DFT calculations were performed with IUPUI start-up funds (J. P and M. N). XRD and EDX analyses were conducted with Hitachi and Bruker instruments purchased using NSF-MRI awards No. MRI-1229514 and MRI-1429241, respectively. R.S. acknowledges Prof. R. Beaulac (Michigan State U.) for helpful discussions.

REFERENCES

1 El-Sayed, M. A. *Acc. Chem. Res.*, 2004, **37**, 326-333.
2 Smith, A. M. and Nie, S. *Acc. Chem. Res.*, 2009, **43**, 190-200.
3 Murray, C. B., Norris, D. J. and Bawendi, M. G. *J. Am. Chem. Soc.*, 1993, **115**, 8706-8715.
4 Hines, M. A. and Guyot-Sionnest, P. *J. Phys. Chem. B*, 1998, **102**, 3655-3657.
5 Peng, X., Manna, L., Yang, W., Wickham, J., Scher, E., Kadavanich, A. and Alivisatos, A. P. *Nature*, 2000, **404**, 59-61.
6 Alivisatos, A. P. *Science*, 1996, **271**, 933-937.
7 Frederick, M. T. and Weiss, E. A. *ACS Nano*, 2010, **4**, 3195-3200.
8 Frederick, M. T., Amin, V. A., Swenson, N. K., Ho, A. Y. and Weiss, E. A. *Nano Lett.*, 2012, **13**, 287-292.
9 Zhou, Y., Wang, F. and Buhro, W. E. *J. Am. Chem. Soc.*, 2015, **137**, 15198-15208.
10 Lawrence, K. N., Dutta, P., Nagaraju, M., Teunis, M. B., Muhoberac, B. B. and Sardar, R. *J. Am. Chem. Soc.*, 2016, **138**, 12813-12825.

11 La Croix, A. D., O'Hara, A., Reid, K. R., Orfield, N. J., Pantelides, S. T., Rosenthal, S. J. and Macdonald, J. E. *Nano Lett.*, 2017, **17**, 909-914.
12 Buckley, J. J., Couderc, E., Greaney, M. J., Munteanu, J., Riche, C. T., Bradforth, S. E. and Brutchey, R. L. *ACS Nano*, 2014, **8**, 2512-2521.
13 Luther, J. M., Law, M., Song, Q., Perkins, C. L., Beard, M. C. and Nozik, A. J. *ACS Nano*, 2008, **2**, 271-280.
14 Scheele, M., Hanifi, D., Zherebetskyy, D., Chourou, S. T., Axnanda, S., Rancatore, B. J., Thorkelsson, K., Xu, T., Liu, Z., Wang, L.-W., Liu, Y. and Alivisatos, A. P. *ACS Nano*, 2014, **8**, 2532-2540.
15 Koole, R., Liljeroth, P., de Mello Donega, C., Vanmaekelbergh, D. and Meijerink, A. *J. Am. Chem. Soc.*, 2006, **128**, 10436-10441.
16 Liang, Y., Thorne, J. E. and Parkinson, B. A. *Langmuir*, 2012, **28**, 11072-11077.
17 Crisp, R. W., Schrauben, J. N., Beard, M. C., Luther, J. M. and Johnson, J. C. *Nano Lett.*, 2013, **13**, 4862-4869.
18 Lawrence, K., Johnson, M., Dolai, S., Kumbhar, A. and Sardar, R. *Nanoscale*, 2015, **7**, 11667-11677.
19 Bayer, M., Hawrylak, P., Hinzer, K., Fafard, S., Korkusinski, M., Wasilewski, Z. R., Stern, O. and Forchel, A. *Science*, 2001, **291**, 451-453.
20 Schedelbeck, G., Wegscheider, W., Bichler, M. and Abstreiter, G. *Science*, 1997, **278**, 1792-1795.
21 Zhao, J., Holmes, M. A. and Osterloh, F. E. *ACS Nano*, 2013, **7**, 4316-4325.
22 Haiming, Z., Ye, Y., Kaifeng, W. and Tianquan, L. *Annu. Rev. Phys. Chem.*, 2016, **67**, 259-281.
23 Wilker, M. B., Shinopoulos, K. E., Brown, K. A., Mulder, D. W., King, P. W. and Dukovic, G. *J. Am. Chem. Soc.*, 2014, **136**, 4316-4324.
24 Han, Z., Qiu, F., Eisenberg, R., Holland, P. L. and Krauss, T. D. *Science*, 2012, **338**, 1321-1324.
25 Kamat, P. V., Tvrdy, K., Baker, D. R. and Radich, J. G. *Chem. Rev.*, 2010, **110**, 6664-6688.
26 Tang, J., Kemp, K. W., Hoogland, S., Jeong, K. S., Liu, H., Levina, L., Furukawa, M., Wang, X., Debnath, R., Cha, D., Chou, K. W., Fischer, A., Amassian, A., Asbury, J. B. and Sargent, E. H. *Nat. Mater.*, 2011, **10**, 765-771.
27 Gur, I., Fromer, N. A., Geier, M. L. and Alivisatos, A. P. *Science*, 2005, **310**, 462-465.
28 Huynh, W. U., Dittmer, J. J. and Alivisatos, A. P. *Science*, 2002, **295**, 2425-2427.
29 Krause, M. M., Mooney, J. and Kambhampati, P. *ACS Nano*, 2013, **7**, 5922-5929.
30 Califano, M., Franceschetti, A. and Zunger, A. *Nano Lett.*, 2005, **5**, 2360-2364.
31 de Mello Donegá, C., Bode, M. and Meijerink, A. *Phys. Rev. B*, 2006, **74**, 085320.
32 Jones, M., Lo, S. S. and Scholes, G. D. *Proc. Nat. Acad. Sci*, 2009, **106**, 3011-3016.
33 Klimov, V. I., Mikhailovsky, A. A., Xu, S., Malko, A., Hollingsworth, J. A., Leatherdale, C. A., Eisler, H. J. and Bawendi, M. G. *Science*, 2000, **290**, 314-317.
34 Del Ben, M., Havenith, R. W. A., Broer, R. and Stener, M. *J. Phys. Chem. C*, 2011, **115**, 16782-16796.
35 Kasuya, A., Sivamohan, R., Barnakov, Y. A., Dmitruk, I. M., Nirasawa, T., Romanyuk, V. R., Kumar, V., Mamykin, S. V., Tohji, K., Jeyadevan, B., Shinoda, K., Kudo, T., Terasaki, O., Liu, Z., Belosludov, R. V., Sundararajan, V. and Kawazoe, Y. *Nat. Mater.*, 2004, **3**, 99-102.

36 Fukunaga, N. and Konishi, K. *Nanoscale*, 2015, **7**, 20557-20563.
37 Chen, P. E., Anderson, N. C., Norman, Z. M. and Owen, J. S. *J. Am. Chem. Soc.*, 2017, **139**, 3227-3236.
38 Boles, M. A., Ling, D., Hyeon, T. and Talapin, D. V. *Nat. Mater.*, 2016, **15**, 141-153.
39 Teunis, M. B., Dolai, S. and Sardar, R. *Langmuir*, 2014, **30**, 7851-7858.
40 Anderson, N. C., Hendricks, M. P., Choi, J. J. and Owen, J. S. *J. Am. Chem. Soc.*, 2013, **135**, 18536-18548.
41 Fischer, S. A., Crotty, A. M., Kilina, S. V., Ivanov, S. A. and Tretiak, S. *Nanoscale*, 2012, **4**, 904-914.
42 Peng, X. *Adv. Mater.*, 2003, **15**, 459-463.
43 Newton, J. C., Ramasamy, K., Mandal, M., Joshi, G. K., Kumbhar, A. and Sardar, R. *J. Phys. Chem. C*, 2012, **116**, 4380-4389.
44 Dubois, F., Mahler, B., Dubertret, B., Doris, E. and Mioskowski, C. *J. Am. Chem. Soc.*, 2007, **129**, 482-483.
45 Herndon, W. C. *J. Am. Chem. Soc.*, 1973, **95**, 2404-2406.
46 Hoffmann, R. *Rev. Mod. Phys.*, 1988, **60**, 601-628.
47 Kilina, S., Ivanov, S. and Tretiak, S. *J. Am. Chem. Soc.*, 2009, **131**, 7717-7726.
48 Sardar, R., Shem, P. M., Pecchia-Bekkum, C., Bjorge, N. S. and Shumaker-Parry, J. S. *Nanotechnology*, 2010, **21**, 345603-345611.
49 Dolai, S., Nimmala, P. R., Mandal, M., Muhoberac, B. B., Dria, K., Dass, A. and Sardar, R. *Chem. Mater.*, 2014, **26**, 1278-1285.
50 Johnson, B. F. G., Al-Obaidi, K. H. and McCleverty, J. A. *J. Chem. Soc. A*, 1969, 1668-1670.
51 de Lima, G. M., Menezes, D. C., Cavalcanti, C. A., dos Santos, J. A. F., Ferreira, I. P., Paniago, E. B., Wardell, J. L., Wardell, S. M. S. V., Krambrock, K., Mendes, I. C. and Beraldo, H. *J. Mol. Struc.*, 2011, **988**, 1-8.
52 Munro, A. M., Chandler, C., Garling, M., Chai, D., Popovich, V., Lystrom, L. and Kilina, S. *J. Phys. Chem. C*, 2016, **120**, 29455-29462.
53 Grenland, J. J., Lin, C., Gong, K., Kelley, D. F. and Kelley, A. M. *J. Phys. Chem. C*, 2017, **121**, 7056-7061.
54 Al-Salim, N., Young, A. G., Tilley, R. D., McQuillan, A. J. and Xia, J. *Chem. Mater.*, 2007, **19**, 5185-5193.
55 Swafford, L. A., Weigand, L. A., Bowers, M. J., McBride, J. R., Rapaport, J. L., Watt, T. L., Dixit, S. K., Feldman, L. C. and Rosenthal, S. J. *J. Am. Chem. Soc.*, 2006, **128**, 12299-12306.
56 Cottrell, T. L., 1958, **2nd Ed.**
57 Norman, Z. M., Anderson, N. C. and Owen, J. S. *ACS Nano*, 2014, **8**, 7513-7521.
58 Wang, Y., Zhang, Y., Wang, F., Giblin, D. E., Hoy, J., Rohrs, H. W., Loomis, R. A. and Buhro, W. E. *Chem. Mater.*, 2014, **26**, 2233-2243.
59 Jeong, S., Achermann, M., Nanda, J., Ivanov, S., Klimov, V. I. and Hollingsworth, J. A. *J. Am. Chem. Soc.*, 2005, **127**, 10126-10127.
60 Munro, A. M., Jen-La Plante, I., Ng, M. S. and Ginger, D. S. *J. Phys. Chem. C*, 2007, **111**, 6220-6227.
61 Li, H., Brescia, R., Krahne, R., Bertoni, G., Alcocer, M. J. P., D'Andrea, C., Scotognella, F., Tassone, F., Zanella, M., De Giorgi, M. and Manna, L. *ACS Nano*, 2012, **6**, 1637-1647.

62 Mokari, T. and Banin, U. *Chem. Mater.*, 2003, **15**, 3955-3960.
63 Ivanov, S. A., Piryatinski, A., Nanda, J., Tretiak, S., Zavadil, K. R., Wallace, W. O., Werder, D. and Klimov, V. I. *J. Am. Chem. Soc.*, 2007, **129**, 11708-11719.
64 Jin, S., Harris, R. D., Lau, B., Aruda, K. O., Amin, V. A. and Weiss, E. A. *Nano Lett.*, 2014, **14**, 5323-5328.
65 Narukawa, Y., Kawakami, Y., Fujita, S. and Nakamura, S. *Phys. Rev. B*, 1999, **59**, 10283-10288.
66 Feldmann, J., Peter, G., Göbel, E. O., Dawson, P., Moore, K., Foxon, C. and Elliott, R. J. *Phys. Rev. Lett.*, 1987, **59**, 2337-2340.
67 Norris, D. J., Efros, A. L., Rosen, M. and Bawendi, M. G. *Phys. Rev. B*, 1996, **53**, 16347-16354.
68 Kaushik Roy, C., Won Jin, K., Yudhisthira, S., Kwang-Sup, L. and Paras, N. P. *Appl. Plys. Lett.*, 2006, **89**, 051109.
69 Xie, Y., Teunis, M. B., Pandit, B., Sardar, R. and Liu, J. *J. Phys. Chem. C*, 2015, **119**, 2813-2821.
70 Lian, S., Weinberg, D. J., Harris, R. D., Kodaimati, M. S. and Weiss, E. A. *ACS Nano*, 2016, **10**, 6372-6382.
71 Wessels, J. M., Nothofer, H.-G., Ford, W. E., von Wrochem, F., Scholz, F., Vossmeyer, T., Schroedter, A., Weller, H. and Yasuda, A. *J. Am. Chem. Soc.*, 2004, **126**, 3349-3356.

TOC GRAPHIC

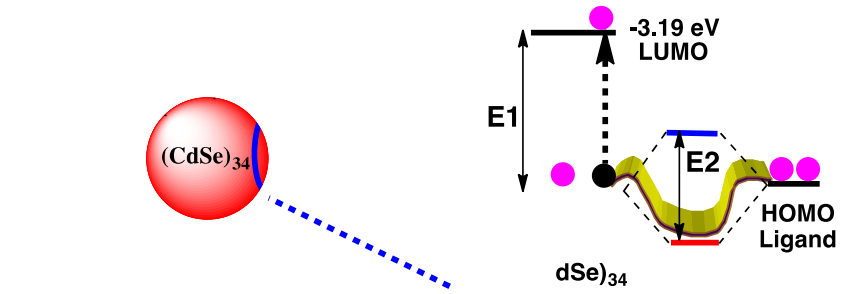
(CdSe)34
-3.19 eV
LUMO
E1
E2
HOMO
Ligand
dSe)34

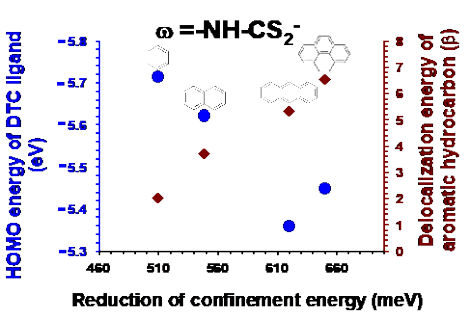
ω =-NH-CS2-
HOMO energy of DTC ligand (eV)
Delocalization energy of aromatic hydrocarbon (β)
Reduction of confinement energy (meV)

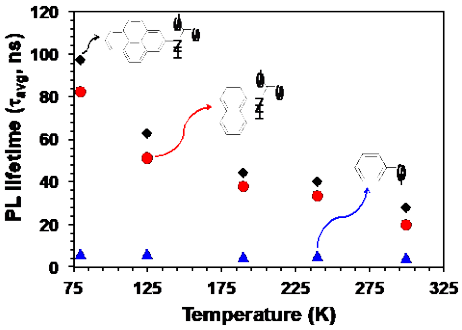
PL lifetime (τavg, ns)
Temperature (K)